

A Model for the Steady-State Photoconductance of an Abrupt p-n Junction Semiconductor Diode Assuming Flat Quasi-Fermi Levels

Keith R. McIntosh

Abstract—A theoretical model for the steady-state photoconductance of an abrupt p-n junction semiconductor diode is presented. It assumes one-dimensional geometry and flat quasi-Fermi levels (QFLs) and involves a numerical integration over electrostatic potential. The flat-QFL model permits the determination of the excess carrier concentration in both quasi-neutral regions from a measurement of a semiconductor's photoconductance, accounting for depletion-region modulation more accurately than its alternatives—particularly for thin samples and low-injection conditions. The model can be generalized to include variable carrier mobilities and to have different intrinsic carrier concentrations in n- and p-type layers.

Index Terms—Carrier lifetime, depletion region, depletion-region modulation (DRM), photoconductance, recombination, space-charge region.

I. INTRODUCTION

PHOTOCONDUCTANCE measurements are widely used to determine semiconductor recombination parameters such as effective lifetime, bulk lifetime, surface recombination velocity, and emitter saturation current. The procedure to determine these parameters involves measuring a sample's excess sheet conductance, converting it to an excess carrier concentration Δn , and analyzing the dependence of Δn on illumination; the analysis can take transient [1], steady-state [2] and generalized [3] forms.

For samples with no lateral variation, the relationship between sheet conductance and carrier concentration is

$$S_{\square} = q \int_0^W [\mu_n(x)n(x) + \mu_p(x)p(x)] dx \quad (1)$$

where q is the elementary charge, W is the width of the semiconductor, $n(p)$ is the electron (hole) concentration, and μ_n (μ_p) is the electron (hole) mobility. This relationship is commonly simplified by assuming constant mobilities and charge neutrality, and by introducing an average carrier concentration

across the width of the semiconductor n_{av} . Combined with (1), these assumptions relate the excess sheet conductance ΔS_{\square} to the excess average carrier concentration Δn_{av} by the explicit analytical equation [1]

$$\Delta S_{\square} = S_{\square L} - S_{\square 0} = q(\mu_p + \mu_n)\Delta n_{av}W \quad (2)$$

where $S_{\square L}$ is the sheet conductance under illumination and $S_{\square 0}$ is the sheet conductance at equilibrium.

When Δn_{av} is approximately equal to Δn in a quasi-neutral region of a sample, it can be used to determine that region's recombination parameters using the analyses in [1]–[3]. But, Δn_{av} can vary significantly from Δn in samples containing a depletion region, whether the depletion region exists at a surface [4]–[8] or at a p-n junction [9], [10], particularly when Δn_{av} or W is small. In such case, an alternative means to determine Δn in the quasi-neutral region(s) is required.

The influence of surface depletion on photoconductance measurements was first recognized by Honma *et al.* [4]. The effect was experimentally established by Hahneiser and Kunst who gave a detailed explanation using numerical simulation [5]. Munakata and Watanabe [6] and Von Aichberger *et al.* [7] developed simple models for transient conditions, where the second of these models permits the determination of the carrier mobility in an inversion channel. Bail *et al.* derived a more sophisticated model for steady-state conditions that involves numerically solving (1) as an integral of electrostatic potential [8].

In the case of a p-n junction, the influence of the depletion region on photoconductance measurements was recognized by Neuhaus *et al.* [9] and Cousins *et al.* [10]. Cousins *et al.* presented a steady-state model that invokes the depletion approximation (DA); it consists of an implicit analytical equation that adds a second term to (2).

In this paper, we extend the approach of Bail *et al.* [8] to semiconductors with a p-n junction. The subsequent model relates ΔS_{\square} to Δn in both the n- and p-type quasi-neutral regions. It accounts for the effect of the depletion region and is relevant to samples of any width. The model assumes that the semiconductor is one-dimensional, that the p-n junction is abrupt, that the p- and n-type regions are uniformly doped, and that the quasi-Fermi levels (QFLs) are flat; it can be generalized to account for variable mobilities and an intrinsic carrier concentration that is different in n- and p-type layers. We also rederive the work of Cousins *et al.* [10], removing

Manuscript received May 15, 2006; revised November 16, 2006. This work was supported by an Australian Research Council Linkage Grant between the Australian National University, SierraTherm Production Furnaces and SunPower Corporation. The review of this paper was arranged by Editor P. Panayotatos.

The author is with the Centre for Sustainable Energy at the Australian National University, Canberra ACT 2600, Australia (e-mail: keith.mcintosh@anu.edu.au).

Digital Object Identifier 10.1109/TED.2006.888719

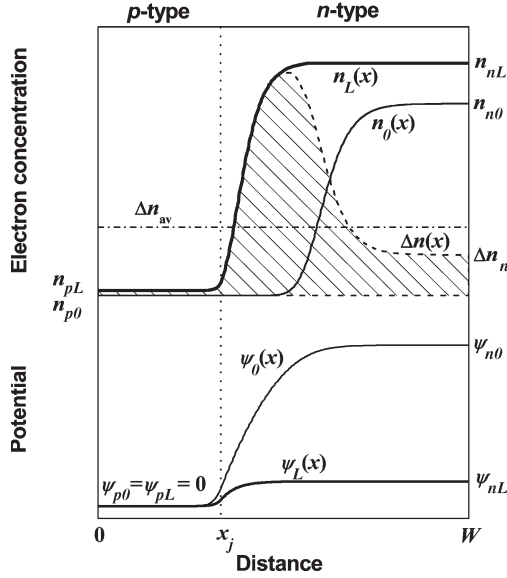


Fig. 1. Electron concentration $n(x)$ and electrostatic potential $\psi(x)$ at equilibrium (0) and under steady-state illumination (L), and the excess electron concentration $\Delta n(x)$. The curves are simulated output from PC1D [11] using the inputs of Example A in Section III.

two assumptions and extending the model to determine Δn in both the n- and p-type layers. The various models are compared using three simulated examples.

The models derived in this paper provide a means to determine Δn in both quasi-neutral regions of a p-n junction semiconductor diode from its photoconductance. They are most relevant when Δn deviates substantially from Δn_{av} , as it occurs when either Δn_{av} or W is small. With respect to the silicon photovoltaic industry—in which the application of photoconductance measurements is ubiquitous—this occurs in wafers when Δn_{av} decreases below $\sim 10^{14} \text{ cm}^{-3}$ or in thin-film cells under any practical illumination intensity.

II. THEORY

A. General Theory

For many photoconductance measurements, it is accurate to assume that a sample's average excess carrier concentration Δn_{av} is equal to the excess carrier concentration in one of the sample's quasi-neutral regions [1]. In such cases, it is appropriate to use (2) to determine Δn from ΔS_{\square} .

The approximation is invalid, of course, when the excess conductance related to a second quasi-neutral region or a depletion region is significant. Fig. 1 presents such an example. While it does not represent a practical device, being thin with n- and p-type regions of similar doping and thickness, the figure provides a clear definition of the problem and the relevant parameters. It plots the electron concentration at equilibrium $n_0(x)$ and under steady-state illumination $n_L(x)$, and their difference: the excess electron concentration $\Delta n(x)$. The figure also defines the excess carrier concentration in the quasi-neutral regions as Δn_n and Δn_p . As implied by “quasi-neutral,” the excess electron and hole concentrations are approximately equal in these regions.

In this example, Δn_{av} departs significantly from both Δn_n and Δn_p , and furthermore, the dependence of Δn_{av} on illumination differs from that of both Δn_n and Δn_p . Consequently, Δn_{av} is not directly related to the recombination rate anywhere in the device.

Both aforementioned reasons are responsible for the departure between Δn_{av} and Δn_n (or Δn_p). As indicated by the integral of $\Delta n(x)$, which relates to the first term of (1), the sheet conductance depends on excess carriers in both quasi-neutral regions and, more significantly, on excess carriers near the depletion region. The first of these reasons applies only when the n- and p-type layers are of a similar thickness and doping concentration—not a common situation in practical devices. The second reason relates to depletion-region modulation (DRM), which has an increasing significance when W and Δn_{av} decrease [10].

DRM is the alteration of a depletion region's characteristics due to injection. When the injection is induced by illumination such that the p-n junction is forward biased, there is a subsequent shrinking of the depletion-region width. As shown in Fig. 1, this change in junction characteristics causes Δn to be greatest in the region that is depleted at equilibrium but not depleted under illumination. Whether one considers the excess carriers to be preferentially “stored” near the edge of the depletion region [9], or the width of the quasi-neutral regions to increase [10], the effect is the same: $\Delta n(x)$ peaks sharply near the edge of the depletion region. Note that $\Delta n(x)$ peaks on the n-type side of the junction (Fig. 1), whereas $\Delta p(x)$ peaks on the p-type side (not plotted).

When Δn_n (or Δn_p) cannot be represented by Δn_{av} , a more sophisticated approach is required to extract it from ΔS_{\square} . While one could utilize simulation packages that solve the full set of semiconductor equations, such as PC1D [11], it is simpler to apply the methods outlined below.

We first describe a method to relate ΔS_{\square} to Δn_p and Δn_n that assumes constant QFLs. We then describe a method that involves the DA (as used by Cousins *et al.* [10]). In both cases, the solutions account for DRM and are applicable to any thickness of p- and n-type layers.

B. Numerical Solution Assuming Constant QFLs

A numerical solution to (1) is now developed based on the approximation of constant QFLs. We first consider the sheet conductance due to electrons—the first term of (1)—converting it from a function of x to a function of electrostatic potential ψ

$$S_{\square n} = q\mu_n \int_0^{\psi_n} \frac{n(\psi)}{d\psi/dx} d\psi \quad (3)$$

where the limits at $x = 0$ and $x = W$ are defined to be $\psi = 0$ and $\psi = \psi_n$. For simplicity, we assume that μ_n is constant for all x (and therefore ψ), although the numerical solution could also be solved for a variable μ_n .

We have followed Aberle *et al.* [12] in defining $\psi = 0$ at $x = 0$, rather than the convention of setting the equilibrium Fermi level to zero. Combined with the assumption of constant

QFLs for electrons ϕ_n and holes ϕ_p , this approach leads to simple expressions for the carrier concentrations [12]

$$n(\psi) = n_i \exp[(\psi - \phi_n)/V_T] = n(0) \exp(\psi/V_T) \quad (4a)$$

$$p(\psi) = n_i \exp[(\phi_p - \psi)/V_T] = p(0) \exp(-\psi/V_T) \quad (4b)$$

where V_T is the thermal voltage and n_i is the intrinsic carrier concentration. These equations assume that n_i is constant throughout the semiconductor. Appendix A shows how both models can be adjusted to account for a different n_i in n- and p-type layers.

Equation (3) also requires an expression for the gradient of the electrostatic potential $d\psi/dx$. As employed by Grove and Fitzgerald to determine surface charge [13] and Nussbaum to determine total recombination [14], we convert Poisson's equation to a first derivative by multiplying both sides by $d\psi/dx$ and integrating, giving

$$\frac{d\psi}{dx} = \sqrt{\frac{-2q}{\epsilon_s} \int [p(\psi) - n(\psi) - N(\psi)] d\psi} \quad (5)$$

where ϵ_s is the permittivity of the semiconductor and $N(\psi)$ is the doping concentration. Only the positive square root is retained because as defined in Fig. 1, $d\psi/dx$ must be positive for all x .

Combining (4) and (5) gives a solution to $d\psi/dx$

$$\frac{d\psi}{dx} = \sqrt{\frac{2qV_T}{\epsilon_s} \left[p(\psi) + n(\psi) + N(\psi) \frac{\psi}{V_T} + C \right]} \quad (6)$$

where C is the constant of integration.

Equation (6) has two solutions: one for the p-type side of the junction where $N(\psi) = N_A$ and $d\psi/dx = 0$ at $\psi = 0$; and one for the n-type side where $N(\psi) = -N_D$ and $d\psi/dx = 0$ at $\psi = \psi_n$. (By this definition of $N(\psi)$, we have assumed an abrupt p-n junction with constant doping concentrations.) Hence, for $\psi \leq \psi_j$

$$\frac{d\psi}{dx} = \sqrt{\frac{2qV_T}{\epsilon_s} \left[p(\psi) - p(0) + n(\psi) - n(0) + N_A \frac{\psi}{V_T} \right]} \quad (7a)$$

and for $\psi \geq \psi_j$

$$\begin{aligned} \frac{d\psi}{dx} \\ = \sqrt{\frac{2qV_T}{\epsilon_s} \left[p(\psi) - p(\psi_n) + n(\psi) - n(\psi_n) - N_D \frac{(\psi - \psi_n)}{V_T} \right]} \end{aligned} \quad (7b)$$

Evidently, an expression for the electrostatic potential at the metallurgical junction ψ_j is required. It is attained by requiring continuity in $d\psi/dx$ at ψ_j by equating (7a) and (7b)

$$\begin{aligned} \psi_j = \frac{V_T}{(N_A + N_D)} \\ * [p(0) + n(0) - p(\psi_n) - n(\psi_n) + N_D \psi_n / V_T]. \end{aligned} \quad (8)$$

To solve (3), we are now left needing expressions for the carrier concentrations at $\psi = 0$ and $\psi = \psi_n$, and an expression for the electrostatic potential in the n-type quasi-neutral region ψ_n . At equilibrium, the carrier concentrations are [15]

$$p(0) = N_A \quad (9a)$$

$$n(0) = n_i^2 / N_A \quad (9b)$$

$$p(\psi_n) = n_i^2 / N_D \quad (9c)$$

$$n(\psi_n) = N_D \quad (9d)$$

and ψ_n equals the equilibrium built-in voltage [15]

$$\psi_n = V_T \ln \left(\frac{N_D N_A}{n_i^2} \right). \quad (10)$$

Under steady-state illumination and assuming flat QFLs, the carrier densities are

$$n(0) = \Delta n_p \quad (11a)$$

$$p(0) = \Delta n_p + N_A \quad (11b)$$

$$n(\psi_n) = \Delta n_n + N_D \quad (11c)$$

$$p(\psi_n) = \Delta n_n \quad (11d)$$

assuming that $\Delta n_n \gg n_i^2 / N_D$ and $\Delta n_p \gg n_i^2 / N_A$.

To determine ψ_n , (11a)–(11d) are combined with (4a)–(4b), to give two equations

$$n(\psi_n) = \Delta n_n + N_D = \Delta n_p \exp[\psi_n / V_T] \quad (12a)$$

$$p(\psi_n) = \Delta n_n = (\Delta n_p + N_A) \exp[-\psi_n / V_T] \quad (12b)$$

that has a quadratic solution for Δn_n in terms of Δn_p

$$\Delta n_n = \left[\sqrt{N_D^2 + 4\Delta n_p(\Delta n_p + N_A)} - N_D \right] / 2. \quad (13)$$

Back substituting (13) into (12a) gives the desired expression for ψ_n

$$\psi_n = V_T \ln \left[\sqrt{1 + \left(\frac{N_A}{\Delta n_p} \right) + \left(\frac{N_D}{2\Delta n_p} \right)^2} + \left(\frac{N_D}{2\Delta n_p} \right) \right]. \quad (14)$$

Thus, the sheet conductance due to electrons can be found by numerically integrating (3) using expressions for $n(\psi)$ from (4a), $d\psi/dx$ from (7), ψ_j from (8), ψ_n from (10) for equilibrium or (14) for illumination, the carrier densities at the limits from (9) for equilibrium or (11) for illumination, and Δn_n from (13) when required for illuminated cases.

There is one complication to numerically solving (3): $d\psi/dx$ is zero at the limits, $\psi = 0$ and $\psi = \psi_n$. This problem is

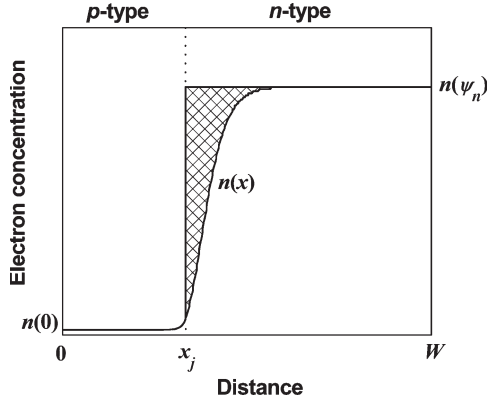


Fig. 2. Cross-hatched area represents the fourth term of (15) for the illuminated example of Fig. 1.

circumvented by using the following rearrangement, which ensures the integrands are always finite

$$\int_0^{\psi_n} \frac{n(\psi)}{d\psi/dx} d\psi = \int_0^{\psi_j} \frac{n(\psi) - n(0)}{d\psi/dx} d\psi - n(0)W_p + n(\psi_n)W_n - \int_{\psi_j}^{\psi_n} \frac{n(\psi_n) - n(\psi)}{d\psi/dx} d\psi \quad (15)$$

where W_p and W_n are the thickness of the p- and n-type layers. For clarity, the final term of (15) is represented as the cross-hatched area in Fig. 2, as simulated for the illuminated case of Fig. 1.

Solving (3)—and an analogous equation for $S_{\square p}$ —provides a solution to the original (1). They can then be used to determine Δn_n and Δn_p from a measured value of ΔS_{\square} .

The method to solving (1) can be somewhat simplified when it is valid to assume that the carrier mobilities are constant, and that the total number of excess holes equals the total number of excess electrons (i.e., there are no trapping effects). In this case, (1) is converted to

$$\Delta S_{\square} = q(\mu_n + \mu_p) \left[\int_0^W n_L(x) dx - \int_0^W n_0(x) dx \right]. \quad (16)$$

The numerical model presented in this section is accurate in all cases where the QFLs are approximately flat. It provides an excess carrier concentration on both sides of the junction; it is applicable to any thickness, thereby being relevant to thin film as well as bulk devices; it can be calculated with simple mathematical programs rather than the complex algorithms required to solve the full set of semiconductor equations; and it permits variable mobilities and a different n_i in the n- and p-type layers. While the model assumes uniform doping profiles in order to find $d\psi/dx$ and ψ_j , it leads to only a small error when applied to samples with a diffused doping profile, as demonstrated by the third example presented below.

Despite these advantages, the flat-QFL model does require numerical integration. The following model manifests as an analytical equation, albeit less accurate.

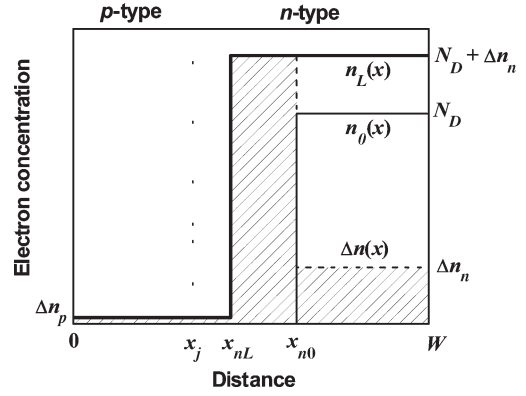


Fig. 3. Electron concentration $n(x)$ and potential $\psi(x)$ at equilibrium (0) and under steady-state illumination (L), and the excess electron concentration $\Delta n(x)$. The curves were determined using the DA for the same input conditions as Fig. 1.

C. Analytical Solution Using the DA

The well-known DA [15] leads to abrupt changes in the carrier concentrations and definable boundaries to the depletion region on the n-type x_n and p-type x_p sides of the metallurgical junction x_j . They are [15]

$$x_j - x_p = \sqrt{\psi_n \frac{2\epsilon_s}{q} \frac{N_A}{N_A(N_A + N_D)}} \quad (17a)$$

$$x_n - x_j = \sqrt{\psi_n \frac{2\epsilon_s}{q} \frac{N_D}{N_D(N_A + N_D)}} \quad (17b)$$

where ψ_n depends on whether the sample is at equilibrium (10) or under steady-state illumination (14).

From Fig. 3, it can be seen that the excess sheet conductance due to electrons is given by

$$\Delta S_{\square n} = q\mu_n [\Delta n_n(W - x_{nL}) + N_D(x_{n0} - x_{nL}) + \Delta n_p(x_{nL} - x_{pL}) + \Delta n_p x_{pL}]. \quad (18)$$

The final two terms of (18) have been separated to enable a simple comparison to the excess sheet conductance due to holes, which is

$$\Delta S_{\square p} = q\mu_p [\Delta n_n(W - x_{nL}) + \Delta n_n(x_{nL} - x_{pL}) + N_A(x_{pL} - x_{p0}) + \Delta n_p x_{pL}]. \quad (19)$$

An expression for ΔS_{\square} is then found by summing (18) and (19)

$$\Delta S_{\square} = q(\mu_n + \mu_p) \Delta n_n(W - x_{nL}) + q(\mu_n + \mu_p) \times N_D(x_{n0} - x_{nL}) + q(\mu_n \Delta n_n + \mu_p \Delta n_p) \times (x_{nL} - x_{pL}) + q(\mu_n + \mu_p) \Delta n_p x_{pL}. \quad (20)$$

This summation has again made use of the DA [15] at equilibrium: $N_D x_{n0} = N_A x_{p0}$; and under illumination: $N_D x_{nL} = N_A x_{pL}$.

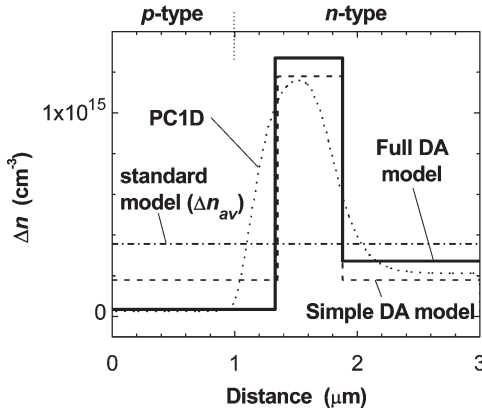


Fig. 4. Comparison of $\Delta n(x)$ as calculated by the full depletion model (20), the simple DA model [10], and the standard solution (2) which is simply an average for $\Delta n(x)$. The solutions to the models are such that the integral of each curve equals that of the PC1D [11] model for the same input conditions. The flat-QFL model cannot be plotted because it involves the calculation of $\Delta n(\psi)$ rather than $\Delta n(x)$; it does, however, result in values for Δn_n and Δn_p that are identical to those of the PC1D model (see Example A in Section III).

Equation (20) is the complete solution to ΔS_{\square} using the DA. It requires values for x_{n0} , x_{nL} , and x_{pL} , all of which can be determined using (17a) or (17b) and the appropriate equation for ψ_n depending on whether the sample is at equilibrium (10) or under illumination (14); and Δn_p is related to Δn_n by (13).

Cousins *et al.* [10] also utilize the DA in their equation for DRM-affected photoconductance. Their solution is the same as (20), but they omit the final two terms and assume that $W \cong W - x_{nL}$. (It could equivalently be said that they set Δn_p to equal Δn_n and omit just the third term.) In doing so, Cousins *et al.* avoid the need to determine Δn_n but limit their model to a sample with one type being much thicker than the other—a satisfactory condition for bulk devices.

Notice that (20) can be converted to the standard solution (2) by omitting the last three terms and assuming $W \cong W - x_{nL}$. As discussed previously, this is valid for samples with one type much thicker than the other and when the influence of DRM is insignificant.

Fig. 4 illustrates the differences between the full DA (20), the simpler version of Cousins *et al.* [10], and the standard solution (2). The figure compares these models for the same input conditions as Fig. 1 (Example A in Section III). In all cases, $\Delta n(x)$ has been determined such that $\Delta S_{\square n}$ for the model is equal to $\Delta S_{\square n}$ for the PC1D solution; consequently, the integral of all curves is equal. This example was specifically chosen to emphasize the differences in the models by using low illumination and assigning the layers with a similar doping and thickness. The standard solution (2) overestimates Δn in the quasi-neutral regions and underestimates it at the p-type edge of the depletion region; the simple DA model of Cousins *et al.* accounts for the DRM but requires $\Delta n_n = \Delta n_p$; and the full DA provides a better representation of $\Delta n(x)$, although it is still significantly different from the PC1D curve at all x . The flat-QFL model cannot be plotted on Fig. 4 because it determines $\Delta n(\psi)$ rather than $\Delta n(x)$. In this example, however, the QFLs are flat and the calculation of Δn_n and Δn_p is consistent with the PC1D model, as demonstrated in the following section.

TABLE I
SUMMARY OF MODELS

Model	Eq. in this paper	Eq. in reference
1. PC1D	—	n.a. in [11]
2. Flat QFL model ^a	(3)–(15) ^c	—
3a. Full DA model ^b	(20)	—
3b. Simple DA model ^b	—	(4) in [8]
4. Standard model	(2)	(1) in [11]

^aQFL: Quasi-Fermi level.

^bDA: Depletion approximation.

^cEquations for ΔS_n ; analogous equations are derived for ΔS_p .

III. COMPARISON OF MODELS

The models, summarized in Table I, are now compared using three simulated examples. The inputs of the examples are chosen to represent (A) a thin silicon sample with flat QFLs, (B) a thin-film silicon solar cell, and (C) a symmetrically diffused silicon wafer. In all cases, the sheet conductance was determined using PC1D [11] over a wide range of illumination levels. The mobilities were constant at $\mu_n = 1200 \text{ cm}^2 \cdot \text{V}^{-1} \cdot \text{s}^{-1}$ and $\mu_p = 400 \text{ cm}^2 \cdot \text{V}^{-1} \cdot \text{s}^{-1}$, and the intrinsic carrier concentration was constant at $n_i = 1.0 \times 10^{10} \text{ cm}^{-3}$. These values were made constant to permit a fair comparison between the models, although in practice, they would vary in the regions of heavy doping. The remaining inputs of relevance are listed in Table II, showing the doping concentrations and thickness of the layers as well as the carrier lifetimes τ , the surface recombination velocity SRV at both surfaces, and the illumination spectrum.

The results of the comparison are presented in Figs. 5–7. They plot the relative error in Δn_n and Δn_p as calculated by the models (subscript “calc”) when compared to those determined by PC1D (no subscript).

Fig. 5 presents the results of Example A, which represents a thin silicon sample with flat QFLs. Flat QFLs were attained by using a uniform generation profile (as results from 1150-nm illumination) and from zero surface recombination. Not surprisingly, the flat-QFL model accurately determines Δn_n and Δn_p at all injection levels (to within 0.25% for Δn_n and 3.9% for Δn_p). The full DA model tends to overestimate both Δn_n and Δn_p , particularly at low injection when DRM is more evident; the simple DA model follows a similar path but is slightly lower due to its approximation that $\Delta n_n = \Delta n_p$; and as described in [10], the standard model becomes increasingly inaccurate for decreasing injection. All models converge with PC1D once both layers are in high injection.

Fig. 6 presents the results of Example B, which represents a thin-film silicon solar cell using dimensions and doping concentrations from [16] under AM1-5g illumination. The trends are similar to Fig. 5, but the error is greater for all models. The flat-QFL model tends to underestimate both Δn_n and Δn_p , increasingly so as injection decreases, but by no more than 5% at the lowest injection tested. The remaining models are very inaccurate at $\Delta n < 10^{15} \text{ cm}^{-3}$. This example illustrates that the flat-QFL model is the only accurate way to analyze photoconductance curves of thin-film solar cells without resorting to a numerical solution of the full set of semiconductor equations.

Fig. 7 presents the results of Example C, which represents a widely used test structure in photovoltaic research: a

TABLE II
INPUTS FOR SIMULATIONS

Example	Represents	Structure	Doping Concentration ^a (cm ⁻³)	Thickness (μm)	τ (μs)	SRV (cm/s)	Illumination Spectrum
A	Thin-film Si with flat QFLs	$p-n$	$10^{16}-10^{15}$	1-2	1	0	1150 nm
B	Thin-film Si solar cell	p^+-n-n^+	$10^{19}-5 \cdot 10^{16}-10^{19}$	0.15-1.5-0.1	0.1	10^4	AM1.5g
C	Test structures used for conventional Si solar cells	n^+-p-n^+	$10^{19}-10^{15}-10^{19}$	1-198-1	100	10^2	AM1.5g

^a Doping concentrations are uniform, except for the n^+ regions in Example C, which are diffusions with an ERFC profile, where the table lists the peak doping concentration and the junction depth.

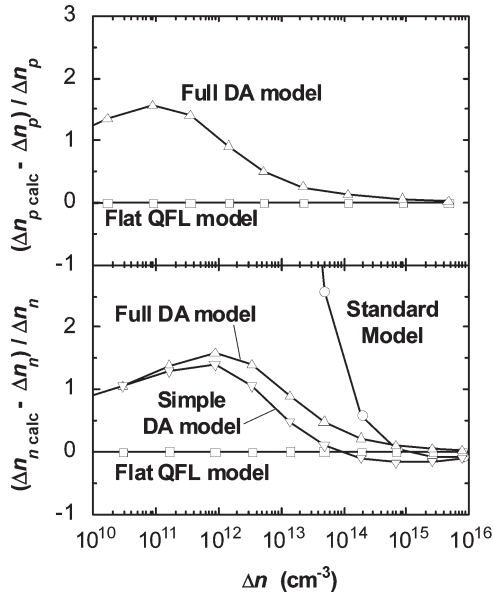


Fig. 5. Relative error in excess carrier concentrations in the quasi-neutral regions as calculated by various models when compared to PC1D solutions. The results relate to Example A, which represents thin-film silicon with flat QFLs.

symmetrically diffused silicon wafer under AM1-5g illumination. In this example, the PC1D value for Δn_p is the average value over the central 190 μm of the p-type layer (since Δn_p varies slightly in the base), and the PC1D value for Δn_n is that at the surface of the n^+ emitter. The figure indicates that the flat-QFL model underestimates Δn at very low injection; this inaccuracy is introduced by the assumption of uniform doping. The flat-QFL model is, however, ~ 5 times more accurate than the DA models, and more accurate still than the standard model. The full and simple DA models give identical results because $W_n \ll W_p$.

This final example is similar to the experimental sample used in [10] who adjusted the sum of the carrier mobilities to make the model consistent with the experiment over the range $\Delta n = 10^{12}-10^{13}$ cm⁻³. Fig. 7 demonstrates that the adjustment of the carrier mobilities may not have been necessary because the DA models overestimate Δn —and hence the effective lifetime—by 5%–50% over this range (for steady-state analyses).

Since the purpose of photoconductance measurements is to determine recombination parameters, this section concludes by comparing the effective lifetime τ_{eff} of each example as determined by the various models. Fig. 8 presents the results in the conventional manner, plotting τ_{eff} as a function of the excess carrier density in the lighter doped quasi-neutral region. Under

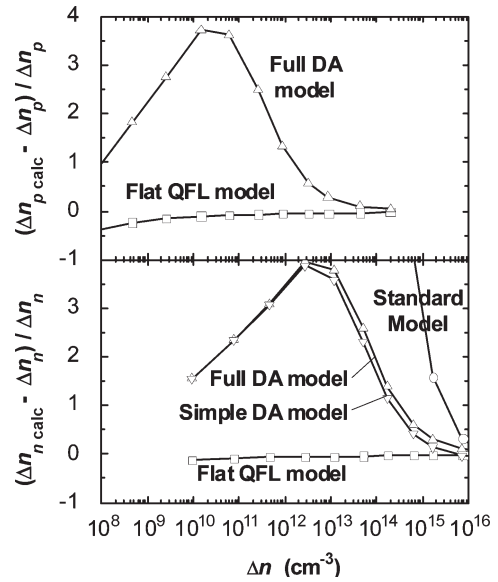


Fig. 6. Relative error in excess carrier concentrations in the quasi-neutral regions as calculated by various models when compared to PC1D solutions. The results relate to Example B, which represents a thin-film silicon solar cell under the AM1-5g spectrum.

steady-state conditions, τ_{eff} is given by the excess carrier concentration divided by the average generation rate of electron-hole pairs [2].

The solid circles in Fig. 8 plot τ_{eff} as determined from the PC1D simulations; the data can be considered the actual τ_{eff} of the three simulated examples. The difference between the actual τ_{eff} and that calculated for the models is similar to the difference in Δn plotted in Figs. 5–7. The trends are not identical, however, but enhanced by the error in Δn being incorporated into both x and y axes. This compounded error highlights the need for accurate analyses of thin samples and low illumination intensities.

It is interesting to note that in Examples A and B, which are both very thin, depletion-region recombination causes τ_{eff} to decline below the bulk lifetime as Δn decreases. (The bulk lifetime is listed in Table II.) The effect also exists in Example C, but is barely identifiable due to the dominance of bulk recombination.

IV. CONCLUSION

The model presented in this paper allows one to determine the excess carrier concentration Δn in both quasi-neutral regions of a p-n junction semiconductor diode from the measurement of its photoconductance. The model assumes that the semiconductor is one-dimensional with flat QFLs, that the

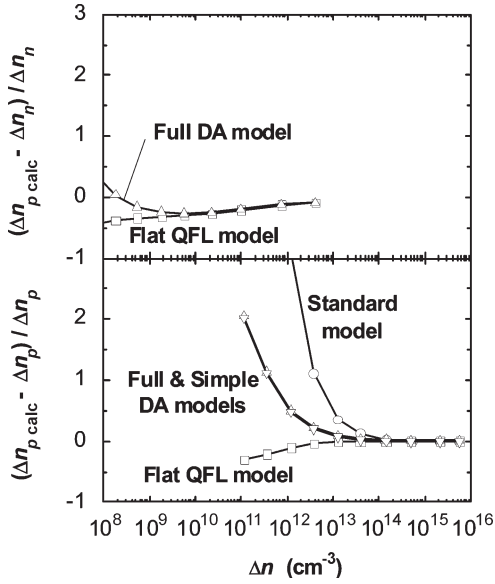


Fig. 7. Relative error in excess carrier concentrations in the quasi-neutral regions as calculated by various models when compared to PC1D solutions. The results relate to Example C, which represents a symmetrically diffused silicon wafer under the AM1-5g spectrum.

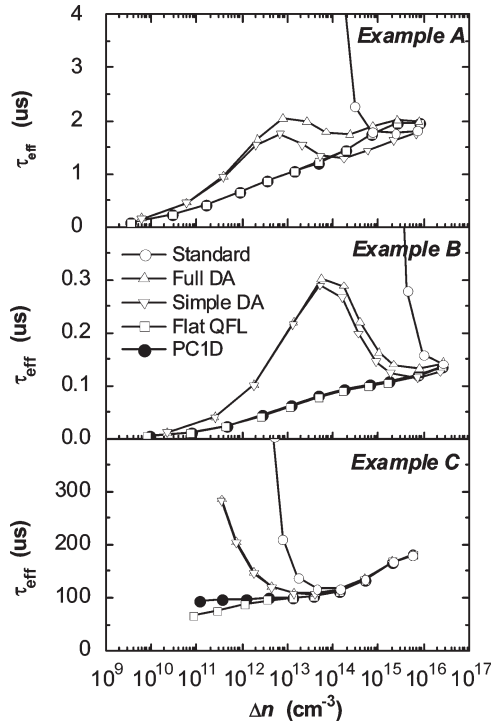


Fig. 8. Effective lifetime plotted against the excess carrier concentration in the lighter doped quasi-neutral region of Examples A, B, and C.

p-n junction is abrupt with uniform doping on either side of the junction, and that the sample is under steady-state illumination. The model was found to be more accurate than its alternatives, particularly when DRM is significant. In practice, it can be used in place of (2) for any steady-state analysis [2] to determine recombination parameters from the relationship between Δn and generation. But being more complicated—it involves a numerical integration and requires more material parameters—the model is most relevant when the accuracy of (2) is insufficient.

With respect to silicon, this occurs in wafers when the excess carrier concentration is below $\sim 10^{14} \text{ cm}^{-3}$, or in thin-film devices under any practical illumination intensity.

APPENDIX

It can be necessary to consider samples where the intrinsic carrier concentration in the n-type layer n_{in} does not equal that in the p-type layer n_{ip} . This might arise in heterojunction structures or heavily doped layers. In such case, (4a) and (4b) are correct on the p-type side of the junction (where ψ is defined to be zero), but on the n-type side, $n(\psi)$ and $p(\psi)$ are given by

$$n(\psi) = (n_{in}/n_{ip}) \cdot n(0) \exp(\psi/V_T) \tag{21a}$$

$$p(\psi) = (n_{in}/n_{ip}) \cdot p(0) \exp(-\psi/V_T). \tag{21b}$$

Consequently, (10) becomes

$$\psi_n = V_T \ln \left(\frac{N_D N_A}{n_{in} n_{ip}} \right) \tag{22}$$

(13) becomes

$$\Delta n_n = \left[\sqrt{N_D^2 + 4(n_{in}/n_{ip})^2 \Delta n_p (\Delta n_p + N_A)} - N_D \right] / 2 \tag{23}$$

and (14) becomes

$$\psi_n = V_T \ln \left[\sqrt{1 + \left(\frac{N_A}{\Delta n_p} \right) + \left(\frac{n_{ip}}{n_{in}} \frac{N_D}{2\Delta n_p} \right)^2} + \left(\frac{n_{ip}}{n_{in}} \frac{N_D}{2\Delta n_p} \right) \right]. \tag{24}$$

For the DA models, (22) or (24) should be used in (17a) and (17b) depending on whether the sample is at equilibrium or under illumination.

REFERENCES

- [1] D. E. Kane and R. M. Swanson, "Measurement of the emitter saturation current by a contactless photoconductivity decay method," in *Proc. IEEE PVSC*, 1985, pp. 578–593.
- [2] R. A. Sinton and A. Cuevas, "Contactless determination of current-voltage characteristics and minority-carrier lifetimes in semiconductors by quasi-steady-state photoconductance data," *Appl. Phys. Lett.*, vol. 69, no. 17, pp. 2510–2512, Oct. 1996.
- [3] H. Nagel, C. Berge, and A. G. Aberle, "Generalized analysis of quasi-steady-state and quasi-transient measurements on carrier lifetimes in semiconductors," *J. Appl. Phys.*, vol. 86, no. 11, pp. 6218–6221, Dec. 1999.
- [4] N. Honma, C. Munakata, and H. Shimizu, "Calibration of minority carrier lifetimes measured with an AC photovoltaic method," *Jpn. J. Appl. Phys.*, vol. 27, no. 7, pp. 1322–1326, Jul. 1988.
- [5] O. Hahneiser and M. Kunst, "Theoretical and experimental study of charge carrier kinetics in crystalline silicon," *J. Appl. Phys.*, vol. 85, no. 11, pp. 7741–7754, Jun. 1999.
- [6] C. Munakata and K. Watanabe, "Charge storage effect in the microwave detected photoconductive decay method," *Jpn. J. Appl. Phys.*, vol. 41, no. 5A, pp. 2796–2800, May 2002.
- [7] S. von Aichberger, O. Abdallah, F. Wunsch, and M. Kunst, "Influence of a space charge region on charge carrier kinetics in silicon wafers," *J. Appl. Phys.*, vol. 91, no. 11, pp. 9147–9150, Jun. 2002.

- [8] M. Bail, M. Schulz, and R. Brendel, "Space-charge region-dominated steady-state photoconductance in low-lifetime Si wafers," *Appl. Phys. Lett.*, vol. 82, no. 5, pp. 757–759, Feb. 2003.
- [9] D. H. Neuhaus, P. J. Cousins, and A. G. Aberle, "Trapping and junction-related perturbations of the effective excess carrier lifetime," in *Proc. 3rd World PVSEC*, 2003, pp. 91–94.
- [10] P. J. Cousins, D. H. Neuhaus, and J. E. Cotter, "Experimental verification of the effect of depletion-region modulation on photoconductance lifetime measurements," *J. Appl. Phys.*, vol. 95, no. 4, pp. 1854–1858, Feb. 2004.
- [11] P. A. Basore and D. A. Clugston, "PC1D version 4 for windows: From analysis to design," in *Proc. 25th IEEE PVSC*, Washington, DC, 1996, pp. 211–214.
- [12] A. G. Aberle, S. Glunz, and W. Warta, "Impact of illumination level and oxide parameters on Shockley-Read-Hall recombination at the Si–SiO₂ interface," *J. Appl. Phys.*, vol. 71, no. 9, pp. 4422–4431, May 1992.
- [13] A. S. Grove and D. J. Fitzgerald, "Surface effects on p-n junctions: Characteristics of surface space-charge regions under non-equilibrium conditions," *Solid State Electron.*, vol. 9, no. 8, pp. 783–806, Aug. 1966.
- [14] A. Nussbaum, "Generation-recombination characteristic behavior of silicon diodes," *Phys. Status Solidi, A*, vol. 19, no. 2, pp. 441–450, Oct. 1973.
- [15] G. W. Neudeck, *The PN Junction Diode*, 2nd ed. Reading, MA: Addison-Wesley, 1989.
- [16] A. G. Aberle, "Progress in evaporated crystalline silicon thin-film solar cells on glass," in *Proc. 4th World Conf. Photovoltaics*, Waikoloa, HI, 2006, pp. 1481–1484.



Keith R. McIntosh received the B.S. degree (with honors) in physics from the University of Sydney, Sydney, Australia, in 1994 and the Ph.D. degree in electrical engineering from the University of New South Wales, Kensington, Australia, in 2001.

In 1995, he taught renewable energy with the University of Zimbabwe, Harare, Zimbabwe and worked with SunPower Corporation, Sunnyvale, CA from 2001 to 2004. In 2005, he became a Research Fellow with the Australian National University, Canberra, Australia, where he leads a research group concern-

ing the optics and surface passivation of photovoltaic solar cells.